

Models in shaping of Milky Way gradients

M. Palla^{1,2}, E. Spitoni^{3,4} and E. Andersson⁵

¹ Sterrenkundig Observatorium, Ghent University, Krijgslaan 281 - S9, 9000 Gent, Belgium e-mail: marco.palla@ugent.be

² INAF – Osservatorio Astronomico di Trieste, Via G.B. Tiepolo 11, 34131 Trieste, Italy

³ Université Côte d’Azur, Observatoire de la Côte d’Azur, CNRS, Laboratoire Lagrange, Bd de l’Observatoire, CS 34229, 06304 Nice cedex 4, France

⁴ Stellar Astrophysics Centre, Department of Physics and Astronomy, Aarhus University, Ny Munkegade 120, DK-8000 Aarhus C, Denmark

⁵ Department of Astronomy and Theoretical Physics, Lund Observatory, Box 43, SE-221 00 Lund, Sweden

Received: 17 July 2022; Accepted: 6 September 2022

Abstract. The great progress in the amount of available observational data for the Milky Way is requiring a great effort in our theoretical interpretation of the Galaxy. In this work, we give some highlights of our theoretical understanding about the shaping of gradients in the Galaxy. In particular, we look at the processes of formation of present-day radial abundance gradients and at the interpretation of the so-called α -bimodality in the context of the two-infall/delayed gas accretion scenario in both the radial and vertical directions. In addition, we provide an example of the advancements in hydrodynamical simulations which are bridging the gap between galactic-scale processes and parsec ones. These models include the complex dynamics of the gas which are necessary to fully explain the evolution of our Galaxy.

Key words. Galaxy: disk, Galaxy: abundances, Galaxy: evolution, methods: numerical

1. Introduction

The distribution of the elements throughout the disc of spiral galaxies generally follows a radial gradient, with metallicity decreasing outward from the galactic centre (e.g. Bresolin & Kennicutt 2015; Magrini et al. 2016; Belfiore et al. 2019). This holds even for the Milky Way (MW), where observables such as HII regions, planetary nebulae (PNe), Cepheids and young-intermediate age open clusters (YOC) (e.g. Balser et al. 2015; Magrini et al. 2017; Stanghellini & Haywood 2018; Kovtyukh et al. 2022 among others) trace this behaviour

in several individual elemental abundances. In general, galactic evolution models find that the Galaxy grows inside-out, i.e. faster in the centre relative to the outskirts in the radial direction (e.g. Schönrich & McMillan 2017). Nonetheless, other processes together with inside-out are often advocated to reproduce the observed gradients (e.g. Grisoni et al. 2018 and references therein).

However, present-day gradients are just part of the challenge to understand the formation and the evolution of the MW. The recent development of large, ground-based spectroscopic surveys (e.g. Gaia–ESO: Gilmore et

al. 2012, APOGEE: Majewski et al. 2017, GALAH: De Silva et al. 2015) has brought a revolution in our view of the MW. In particular, they have allowed us to see a clear bimodal distribution of disc stars in the $[\alpha/\text{Fe}]$ vs. $[\text{Fe}/\text{H}]$ abundance space (e.g. Hayden et al. 2015). The origin of this so-called α -bimodality has received great attention in the last years, with models trying to explain the named high- α and low- α sequences by means of different processes. Among the proposed scenarios (for a summary, see Palla et al. 2022), the hypothesis of a second, delayed gas accretion event originating the low- α sequence is gaining particular consensus by finding support in both MW chemical evolution models (with the two-infall scenario, see e.g. Spitoni et al. 2019; Palla 2021) and many MW-like simulations (e.g. Grand et al. 2018; Buck 2020).

Another revolution in Galactic astronomy has been possible thanks to the advent of the *Gaia* satellite (Gaia collaboration 2016, 2018, 2022), which is providing for billions of stars exquisite orbital information.

The benefit of coupling chemical and orbital properties of stars is of extreme importance to capture the past history of the different components of our Galaxy (see, e.g. Helmi 2020). For the Galactic disc, the cross-matching between spectroscopic surveys and *Gaia* data has enabled us to analyse the distribution of the high- α and low- α sequences also in the vertical direction. In turn, this provide a further test for the mechanisms of formation of our disc, with models generally suggesting an upside-down scenario, i.e. old, high- α stars formed in a thicker, kinematically hot component and low- α in thinner, kinematically cold one (e.g. Bird et al. 2013).

In tandem with the progress regarding the amount and quality of these data, improvements in computational power and numerical methods have led to hydrodynamical simulations now reaching tens of parsec in spatial resolution. Furthermore, simulations resolving individual stars have started to become available (see, e.g. Emerick et al. 2018; Andersson et al. 2020; Hirai et al. 2021; Gutcke et al. 2021; Hislop et al. 2022). This relieves many of the limitations that come with sub-grid modelling

(Somerville & Davé 2015; Naab & Ostriker 2017). Therefore, the gap between galactic and parsec scale processes is starting to be explored.

In this work, we will provide some examples of the theoretical progresses we are making in these last years in the above mentioned fields. In particular, in Section 2 we will discuss the formation of MW radial gradients and the α -bimodality in the MW disc. In Section 3, we will discuss the formation of stellar vertical distributions in the disc of the Galaxy. In Section 4, we will present some of the progress made by state-of-the-art simulations in explaining galactic chemical evolution. Finally, in Section 5 we summarise the key points of the previous sections.

2. MW disc radial gradients and $[\alpha/\text{Fe}]$ bimodality

To probe the observed radial abundance variations in the MW disc, Palla et al. (2020) built a multi-zone chemical evolution model for the Galactic disc based on the two-infall model framework (e.g. Chiappini et al. 1997). In this scenario, the Galactic disc forms out of two sequential gas accretion episodes, with an age gap that has been highly debated in the last years (e.g. Spitoni et al. 2019).

In this paper we explore the effects of several model physical parameters, such as different inside-out laws for gas accretion, efficiencies of star formation and radial gas inflows during the second infall episode, different age gaps between the two gas accretion events and profiles of the ratio between present-day, total (gas+stars) surface densities produced by the two infall episodes. For further description of the model details, we address the reader to Palla et al. (2020).

In Fig. 1, we see the effects of inside-out mechanism, variable efficiency of star formation (decreasing with radius) and several prescriptions for radial gas flows (i.e. constant velocity, radius dependent velocity, radius and time dependent velocity) in setting the present-day abundance gradients.

In this Figure, the different model setups are compared with the observed present-day radial

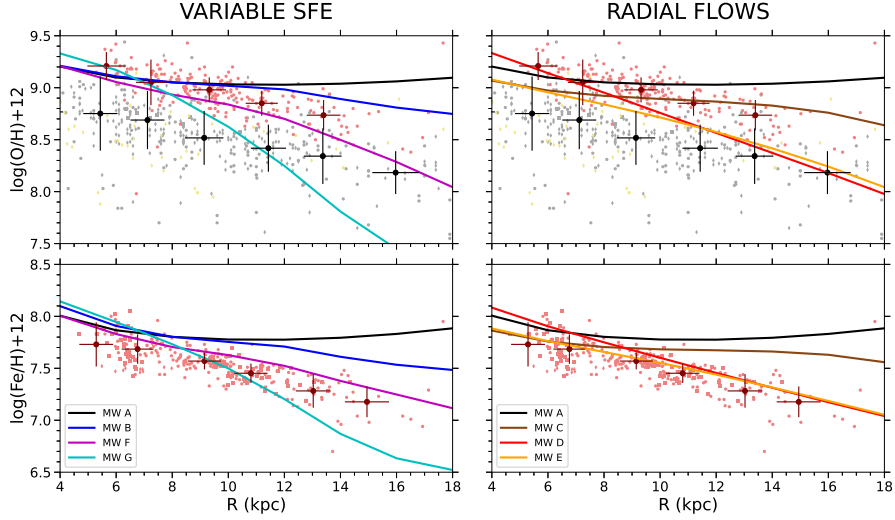


Fig. 1. Observed and predicted abundance gradients along the thin disc. Black points with error bars represent data bins with associated rms for HII regions and PNe (data from Costa et al. 2004; Esteban et al. 2005; Rudolph et al. 2006; Balser et al. 2015; Stanghellini & Haywood 2018), while the red points with error bars refer to Cepheids and YOC (data from Luck & Lambert 2011; Genovali et al. 2015; Magrini et al. 2017). The shift between nebular and stellar data can be partly attributed to an underestimation in some HII region abundances due to temperature fluctuations (see Méndez-Delgado et al. 2022)

. Model A includes only the inside-out mechanism (Romano et al. 2000). Model C, D and E in the right panels add radial gas inflows with different prescriptions for the flow speed (constant, radial dependent and both radial and time dependent, respectively). Models B, F and G in the left panels add radial variable star formation efficiency (combined with different radial gas flows prescriptions for models F and G).

abundance gradients from Cepheids, YOC, HII regions and PNe. The Figure shows that the inside-out mechanism cannot be considered as the main responsible for radial gradients formation. In fact, the predicted gradients for both elements produced on short timescales (e.g. O) and long timescales (e.g. Fe) are too flat to match the observations. This holds either implementing the well adopted inside-out law by Romano et al. 2000 (black solid lines in Fig. 1) or using flatter or steeper laws, with values in these ranges:

$$\tau(R) = ([0.75, 1.25] R/\text{kpc} + [0.997, -3.003]) \text{Gyr}. \quad (1)$$

Therefore, either variable efficiency of star formation (with values between 5 and 0.1 Gyr^{-1} , instead of a constant 1 Gyr^{-1} efficiency) or radial gas inflows (with velocities v between 0 and 4 km s^{-1} , e.g. Vincenzo & Kobayashi

2020) are needed to increase the gradient slope.

Palla et al. (2020) also looked at the star formation rate and gas radial density gradients to disentangle the degenerate solutions that reproduce the observed abundance gradients. In this way, they found that a combination of variable efficiency of star formation and mild ($v \sim 1 \text{ km s}^{-1}$), constant radial gas inflows best reproduces the observed radial trends.

As a second step, Palla et al. (2020) compared their best model in explaining the present-day gradients with APOGEE data from Hayden et al. (2015), sampling the $[\alpha/\text{Fe}]$ vs. $[\text{Fe}/\text{H}]$ diagram on a wide range of Galactocentric distances (3-15 kpc). As done for the abundance gradients, they looked at the effects of different model parameters on the predictions. In particular, they tested dif-

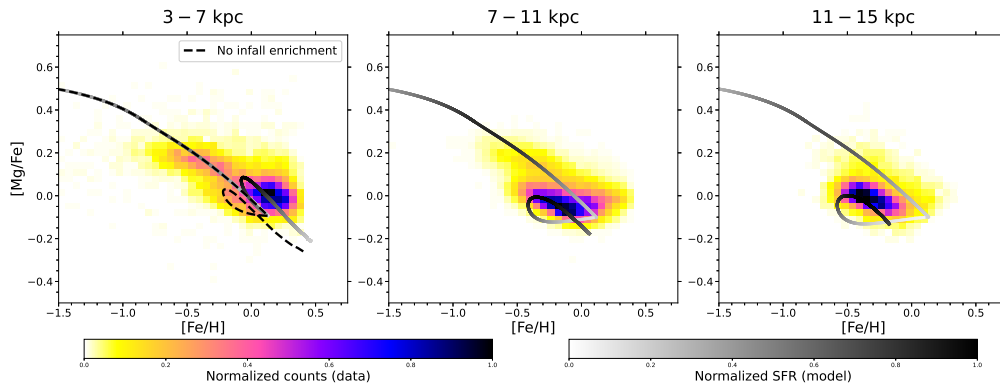


Fig. 2. $[\text{Mg}/\text{Fe}]$ vs. $[\text{Fe}/\text{H}]$ abundance ratios for the best model for the MW disc compared to APOGEE data. Left, central and right panels show the models and data in the ranges $3 < R/\text{kpc} < 7$, $7 < R/\text{kpc} < 11$ and $11 < R/\text{kpc} < 15$, respectively. The left panel also shows a model without enrichment in the second infall episode (dashed line) to highlight the effect of gas enrichment on abundance patterns. The left colorbar indicates the normalised counts of data, while the right colorbar indicates the normalised SFR predicted by the model at a certain $[\text{Mg}/\text{Fe}]$ and $[\text{Fe}/\text{H}]$.

ferent age gaps between the two gas accretion events and different radial profiles of the ratio between surface mass densities produced by these two. It is worth reminding that such variations have marginal effects on present-day gradients, with the slopes barely affected.

The authors found that a delay larger than 3 Gyr (i.e. 3.25 Gyr) between the first and the second gas accretion events, as well as a ratio between surface densities produced by second and first infall steeply increasing with radius (~ 2.5 at 4 kpc, ~ 10 at 14 kpc), are required to reproduce the behaviour of the α -bimodality at different radii. The claim of a larger delay between the first and the second infall relative to the original version by Chiappini et al. (1997) extends to a wider range of galactocentric radii the conclusion of Spitoni et al. (2019), who proposed a delay of ~ 4 Gyr to explain $[\alpha/\text{Fe}]$ and asteroseismic ages in a local stellar sample. The steep increase with radius of the ratio between second and first infall surface densities also represents a novelty in the two-infall model framework, as previous papers (e.g. Grisoni et al. 2017) adopted a ratio decreasing with radius. The need for the increasing trend is explained in terms of the progressively larger low- α to high- α star counts towards larger

radii (see also Queiroz et al. 2020): in fact, in the model the first and second infall episodes originate the high- α and the low- α sequences, respectively.

We see in Fig. 2 central and right panels that such a model set-up allows a good agreement between predicted and observed abundance trends in the “solar” (7-11 kpc) and outer (11-15 kpc) disc regions. Concerning the innermost disc region (Fig. 2 left panel) instead, we reach a better agreement with the observed $[\alpha/\text{Fe}]$ vs. $[\text{Fe}/\text{H}]$ trend if all the gas is enriched at a level of $[\text{Fe}/\text{H}]=-0.5$ dex during the second infall episode, with an abundance pattern resembling that of the high- α sequence. Several hypotheses can be made for the origin of this infall enrichment. In particular, this can be the effect of the mixing between the gas leftover from the formation of the Galactic halo or Galactic bulge/bar and the primordial extragalactic infalling gas.

Spitoni et al. (2021) also tested these claims still in the context of the two-infall model, but in a Bayesian framework, adopting updated APOGEE data by Ahumada et al. (2020). In particular, the authors performed a Monte Carlo Markov Chain (MCMC) iteration on models parameters to quantitatively find the

best fit model to APOGEE data. For further descriptions on the fitting procedure, we refer the reader to Spitoni et al. (2021).

Despite of the slightly different dataset and model details (i.e. massive stars stellar yields from François et al. 2004 instead of Kobayashi et al. 2006), they confirmed the main findings of the previous analysis on the $[\alpha/\text{Fe}]$ sequence at different radii, with age gaps above 3 Gyr at all radii and second to first infall total surface density ratio increasing with radius. The enrichment in the second gas accretion was also confirmed, and this can be easily connected with several claims coming from hydrodynamical simulations of MW-like galaxies (e.g. Khoperskov et al. 2021).

However, at variance with suggestions from several simulations (e.g. Agertz et al. 2021), the discussed chemical evolution studies found that gas from Gaia-Enceladus-Sausage (GES) merger is not likely to be the responsible of the enrichment of the gas accreting onto the MW disc. In fact, by running a specific chemical evolution model for GES progenitor (see Vincenzo et al. 2019 for details) and applying a gas mixture including the outcome of this model to the infall, the resulting $[\alpha/\text{Fe}]$ ratios are too low to reproduce the observed bimodality in the inner Galactic regions.

3. Disc bimodality in the vertical $[\text{Mg}/\text{Fe}]$ distribution

In the discussed studies in Section 2 and in some other ones (see e.g., Spitoni et al. 2019b, 2020, 2022a) the high- α versus low- α disc bimodality was analysed making predictions just for projected quantities on the Galactic plane. In Spitoni et al. (2022b), this impasse was broken presenting the vertical distribution of chemical elements assuming simplified dynamical prescriptions in the chemical evolution models.

In fact, in order to better understand the processes that affected and shaped the formation and evolution of the Galactic disc, it is very important to compare model predictions also with the observed vertical $[\alpha/\text{Fe}]$ distribution of stars at different heights above the Galactic plane.

Vincenzo et al. (2021) highlighted the presence of a bimodality in the vertical $[\alpha/\text{Fe}]$ distribution of APOGEE data that can be well modelled adopting a double Gaussian stellar distribution highlighting that the dichotomy observed in the $[\alpha/\text{Fe}]$ ratios near the solar radius is an intrinsic property of the stellar disc components, not an artefact of over-representing thick-disc stars. Beside the chemical signatures, the orbital properties of stars and in particular the change of dynamical actions over time constrain the main physical processes that have shaped the observed stellar distribution. For instance, Gandhi & Ness (2019) found that at all ages, the high- α and low- α components are dynamically distinct and that selections in the actions space can provide an efficient method to separate distinct dynamical populations.

In order to provide predictions on the vertical distribution of the chemical elements, Spitoni et al. (2022b) integrated stellar orbits for different simple stellar populations (SSPs) born at different evolutionary times subject to the *MWPotential2014* gravitational potential of Bovy (2015).

They considered i) the vertical action J_z associated to the different SSPs as an integral of motion, ii) the J_z vs. stellar ages relation found by Ting & Rix (2019). In fact, Ting & Rix (2019) interpreted the distribution of the vertical actions J_z of red-clump stars in APOGEE as a combination of the vertical action at birth plus the subsequent heating, proposing an analytical expression of J_z vs. stellar ages τ . This relation computed in the solar vicinity can be written as:

$$J_z = 0.91 + 1.81 \cdot \left(\frac{\tau}{1\text{Gyr}} \right)^{1.09} \text{ [kpc km s}^{-1}\text{]}. \quad (2)$$

Hence, for each SSP, beside the chemical composition predicted by the Spitoni et al. (2021) model, Spitoni et al. (2022b) provided orbital properties, as the maximum vertical heights $|z_{\text{max}}|$. The model predictions for Mg and Fe vertical distribution were compared with APOGEE data (Ahumada et al. 2020). In particular, they looked at stars with Galactocentric distances between 6 and 10 kpc

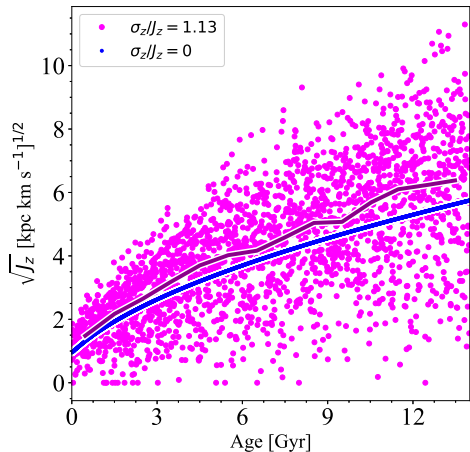


Fig. 3. The Ting & Rix (2019) relation between the vertical action J_z and the age, computed at 8 kpc is indicated with the blue line. The “new” vertical action $J_{z,new}$ (see eq. 5 in Spitoni et al. 2022b) including observed dispersion of $\sigma_{J_z} = 1.13 \cdot J_z$ proposed by Gandhi & Ness (2019) for the thick disc is reported with the magenta points. The solid dark-magenta line indicates the medians values.

as computed by Leung & Bovy 2019, for which stellar maximum disc height $|z_{max}|$ as computed by Mackereth & Bovy (2018) are also provided in the value-added astroNN¹ catalogue.

In Spitoni et al. (2022b), they presented predictions on the $[Mg/Fe]$ vs. $|z_{max}|$ distributions also assuming a dispersion in model results by adding, at each Galactic time t , a random error - which follows a Gaussian distribution - to the vertical action J_z of Ting & Rix (2019) associated to the formed SSP at the same time. They explored the following dispersion values: $\sigma_{J_z}/J_z = 0.5$ and $\sigma_{J_z}/J_z = 1$.

In this paper, we show predictions on the $[Mg/Fe]$ vs. $|z_{max}|$ distributions assuming $\sigma_{J_z}/J_z = 1.13$, exactly the value that has been presented by Gandhi & Ness (2019) for the thick disc phase. In Fig. 3, we show the Ting & Rix (2019) relation between the vertical action J_z and the age. We also include the “new” vertical action $J_{z,new}$ (see eq. 5 in Spitoni et al.

¹ <https://data.sdss.org/sas/dr16/apogee/vac/apogee-astroNN>

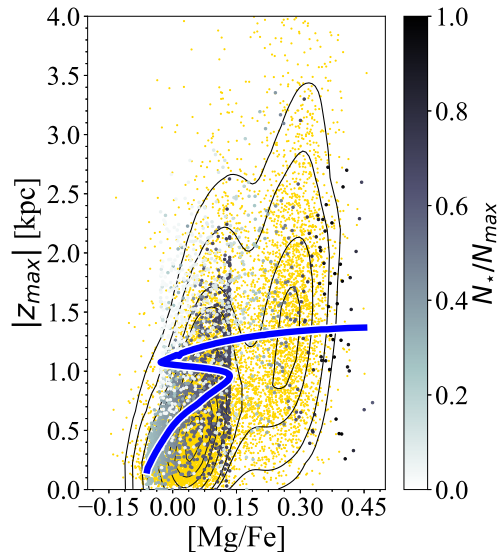


Fig. 4. The vertical maximum orbital excursion z_{max} vs. $[Mg/Fe]$ in the Galactic region centered at the solar position. The yellow points indicate APOGEE $[Mg/Fe]$ abundance ratio (Ahumada et al. 2020) vs. $|z_{max}|$ (within Galactocentric region between 6 and 10 kpc and $|z| < 2$ kpc as reported in the astroNN catalogue). The contour lines enclose fractions of 0.95, 0.90, 0.75, 0.60, 0.45, 0.30, 0.20 and 0.05 of the total number of observed stars. With the blue line we report model predictions by Spitoni et al. (2022b). The colour coding represents the total number of stars predicted in that region considering a Gaussian standard deviation assuming $\sigma_{J_z} = 1.13 \cdot J_z$ as found in Gandhi & Ness (2019) for the thick disc stars.

2022b) including the observed dispersion of $\sigma_{J_z} = 1.13 \cdot J_z$ proposed by Gandhi & Ness (2019) for the thick disc.

In Fig. 4 we show instead our model predictions in the $[Mg/Fe]$ vs. $|z_{max}|$ plane. With the blue line, we show Spitoni et al. (2022b) results assuming no dispersion in J_z . Here, we note the neat transition between high- α and low- α sequence stars. Moreover, it is possible to appreciate that the distributions of the predicted SSPs in the $|z_{max}|$ vs. $[Mg/Fe]$ space including the observed dispersion of $\sigma_{J_z} = 1.13 \cdot J_z$, show the presence of the disc dichotomy signature, in good agreement with data. In fact, the spread in the data is nicely

reproduced using in the calculation of J_Z the dispersion proposed by Gandhi & Ness (2019) for the thick disc. Furthermore, our results are consistent with Spitoni et al. (2022b) findings where $\sigma_{J_z} = 1 \cdot J_Z$ and $\sigma_{J_z} = 0.5 \cdot J_Z$ were considered.

In conclusions, the signatures i) of a delayed gas infall and ii) the hiatus in the star formation history of the Galaxy are imprinted both in the $[\text{Mg}/\text{Fe}]$ vs. $[\text{Fe}/\text{H}]$ relation (see Section 2) and in vertical distribution of $[\text{Mg}/\text{Fe}]$ abundances in the solar vicinity.

4. Chemo-dynamical evolution in hydrodynamical simulations with individual stars

The chemo-dynamical processes which are relevant for setting abundance trends in galaxies are starting to be explored through the use of state-of-the-art hydrodynamical simulations (see e.g., Agertz et al. 2021; Buck et al. 2021; Bellardini et al. 2022). These models trace complex gas flows (such as galactic fountains and moving gas clouds in the circumgalactic medium) which can redistribute chemically enriched material, and consequently affect the evolution of abundance gradients. Furthermore, the chaotic assembly history of galaxies in a cosmological framework plays an important role for features in the abundance space (Renaud et al. 2021).

With recent improvements of the aforementioned class of models, the chemical evolution for the majority of elements can be traced (Andersson et al., in prep). Hydrodynamic simulations can now include models for the stellar evolution and kinematics of individual stars (Andersson et al. 2020), significantly improving the modelling of the injection of energy and chemically enriched material into the interstellar medium surrounding a given star. To achieve this, stellar feedback is modelled star-by-star, accounting for stellar winds, as well as core-collapse and type Ia SNe.

Fig. 5 shows the star formation rate (SFR, top panel) and the gas outflow rate \dot{M}_g (bottom panel) for a Wolf-Lundmark-Melotte (WLM) galaxy analogue simulated with a star-by-star

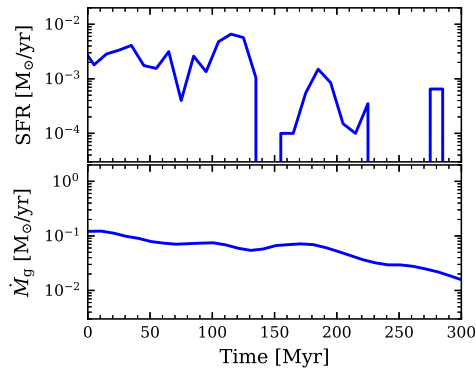


Fig. 5. *Top:* Star formation rate as function of time for a simulation of a WLM-like galaxy. *Bottom:* The gas mass outflow rate as function of time. While the star formation rate is subject to periods of quiescence, the outflow rate is expelled at a stable rate.

model (details in Andersson et al., in prep). Both quantities are displayed as function of time for the final 300 Myr of the simulation, which is preceded by 400 Myr of evolution to achieve a quasi-stable gas cycle. Note that the SFR is computed in 10 Myr time-bins, while \dot{M}_g is computed through a 9 kpc (roughly equal to 20% of the virial radius) spherical shell with a thickness of 2 kpc. Notably, the gas mass lost in outflows exceeds that consumed by star formation by roughly 2 orders of magnitude. This implies a mass loading factor of ~ 100 , in agreement with both semi-analytical models (Somerville & Davé 2015), and estimates from observations (Chisholm et al. 2017) for galaxies in this mass range.

The chemical composition is tracked by advecting metals with the gas flow, and letting stars inherit it. Stars return chemically processed material, using pre-computed yields (Pignatari et al. 2016; Ritter et al. 2018). Elements are selected at initialization (to alleviate computational cost), and in this simulation C, N, O, Mg, Si, Mn, Fe and Ba are included. Fig. 6 shows the loading factors of N, Mg and Mn, defined as

$$\eta_{Z_i} = \frac{\dot{Z}_i}{\dot{y}_{Z_i}}, \quad (3)$$

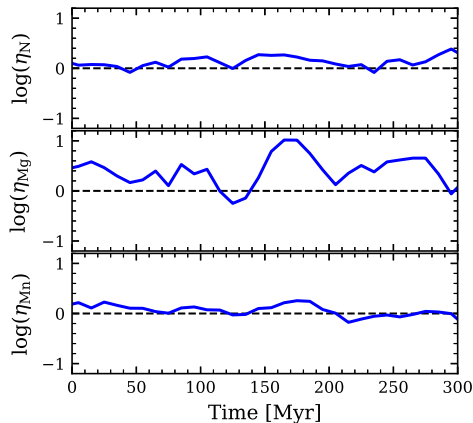


Fig. 6. The logarithm of loading factor for individual elements as function of time, showing N in the top panel, Mg in the central panel, and Mn in the bottom panel. The dashed lines indicate a loading factor of unity, and is meant to guide the reader.

where \dot{Z}_i is the mass outflow rate and \dot{y}_{Z_i} is the yield rate, both for a given element. \dot{Z}_i is computed at the same location as \dot{M}_g , considering only the mass of the given element. This loading factor provides an estimate of how efficiently an element is ejected from the galaxy.

Fig. 6 shows that elements that are injected by highly energetic and spatially correlated feedback channels (e.g., Mg produced in core-collapse SNe) have significantly higher loading factor, compared to other sources of feedback (e.g., stellar winds expelled during the asymptotic giant branch phase). We see this by comparing the top (N) and middle (Mg) panels of Fig. 6, where the loading factor of Mg is shown to exceed that of N by up to 1 dex. Furthermore, expulsion in energetic events alone does not seem to drastically affect the loading factor, as Mn (expelled primarily in type Ia SNe) does not show signs of higher loading factor compared to N. Likely, the excess in Mg loading factor is also driven by the clustered nature of core-collapse SNe, which generates chimneys that funnel material out of the galaxy.

That the galactic wind is not chemically homogeneous has implications for chemical

evolution models, and likely plays a part in setting the scatter observed in chemical abundance trends. In fact, it was shown by Yates et al. (2021) that boosting the material ejected by SNe produce results in better agreement with observed trends. In larger galaxies where outflows vary with galactocentric distance, variations in loading factors for individual elements likely affects their abundance gradient.

5. Summary and conclusions

The great wealth of data released in the last years entice a deeper theoretical understanding of the evolution of the Milky Way (MW).

In this work, we highlight what is the current state of understanding of the MW disc radial and vertical trends in a certain model framework (i.e. the two-infall model). Moreover, we give an example of the effort that state-of-the-art hydrodynamical simulations are making in bridging the gap between galactic and smaller scale processes.

In particular, the main points can be summarised as follows:

- the inside-out formation of the disc must be assisted by additional processes (i.e. variable efficiency of star formation and radial gas inflows) to explain the present-day gradients. The behaviour of the $[\alpha/\text{Fe}]$ bimodal distribution at different radii is well explained by models in which the Galaxy formed out of two main gas accretion episodes, with a significant age gap in between. An enrichment in the second gas accretion for the inner parts of the galaxy is also suggested in this context;
- the vertical distribution of the $[\text{Mg}/\text{Fe}]$ abundance ratio predicted by the two-infall model (including the observed dispersion in the vertical action estimates), shows the presence of the disc dichotomy signature, in good agreement with data. The signature of the hiatus in the star formation history - due to a delayed infall of gas - is imprinted in the vertical distribution of $[\text{Mg}/\text{Fe}]$ abundances in the solar vicinity;

- state-of-the-art hydrodynamical simulations including star-by-star models for stellar feedback and enrichment find that different elements are expelled at different efficiencies. In particular, elements associated with core-collapse SNe have metal loading factors which can be several times higher compared to those from AGB winds and type Ia SNe. These differences likely have an impact on the evolution of abundance gradients.

Acknowledgements. M.P. received funding from the European Research Council (ERC) under the European Union’s Horizon 2020 research and innovation programme DustOrigin (ERC-2019-StG-851622).

E.S. received funding from the European Union’s Horizon 2020 research and innovation program under SPACE-H2020 grant agreement number 101004214 (EXPLORE project). Funding for the Stellar Astrophysics Centre is provided by The Danish National Research Foundation (Grant agreement no.: DNR106).

E.A. acknowledge financial support from the Knut and Alice Wallenberg Foundation and computer resources from Swedish National Infrastructure for Computing (projects SNIC 2021/5-111, SNIC 2021/6-87 and SNIC 2021/6-85)

References

- Agertz, O., Renaud, F., Feltzing, S., et al. 2021, *MNRAS*, 503, 5826
- Ahumada, R., Prieto, C. A., Almeida, A., et al. 2020, *ApJS*, 249, 3
- Andersson, E. P., Agertz, O., & Renaud, F. 2020, *MNRAS*, 494, 3328
- Balsler, D. S., Wenger, T. V., Anderson, L. D., Bania, T. M., 2015, *ApJ*, 806, 199
- Belfiore, F., Vincenzo, F., Maiolino, R., Matteucci, F., 2019, *MNRAS*, 487, 456
- Bellardini, M. A., Wetzell, A., Loebman, S. R., et al. 2022, arXiv:2203.03653
- Bird, J. C., Kazantzidis, S., Weinberg, D. H., et al. 2013, *ApJ*, 773, 43
- Bovy, J. 2015, *ApJS*, 216, 29
- Bresolin, F., Kennicutt, R. J. 2015, *MNRAS*, 454, 3664
- Buck, T. 2020, *MNRAS*, 491, 5435
- Buck, T., Rybizki, J., Buder, S., et al. 2021, *MNRAS*, 508, 3365
- Chiappini, C., Matteucci, F., Gratton, R., 1997, *ApJ*, 477, 765
- Chisholm, J., Tremonti, C. A., Leitherer, C., et al. 2017, *MNRAS*, 469, 4831
- Costa, R. D. D., Uchida, M. M. M., Maciel, W. J., 2004, *A&A*, 423, 199
- De Silva, G. M., et al., 2015, *MNRAS*, 449, 2604
- Emerick, A., Bryan, G. L., & Mac Low, M.-M. 2018, *ApJ*, 865, L22
- Esteban, C., Garcia-Rojas, J., Peimbert, M., Peimbert, A., Ruiz, M. T., Rodriguez, M., Carigi, L., 2005, *ApJ*, 618, L95
- François, P., Matteucci, F., Cayrel, R., et al. 2004, *A&A*, 421, 613
- Gaia Collaboration, 2016, *A&A*, 595, A2
- Gaia Collaboration, 2018, *A&A*, 616, A1
- Gaia Collaboration, 2022, *A&A*, in press
- Gandhi, S. S. & Ness, M. K. 2019, *ApJ*, 880, 134
- Genovali, K. et al., 2015, *A&A*, 580, A17
- Gilmore, G. et al., 2012, *Messenger*, 147, 25
- Grand, R. J. J. et al., 2018, *MNRAS*, 474, 3629
- Grisoni, V., Spitoni, E., Matteucci, F., et al. 2017, *MNRAS*, 472, 3637
- Grisoni, V., Spitoni, E., Matteucci, F., 2018, *MNRAS*, 481, 2570
- Gutcke, T. A., Pakmor, R., Naab, T., et al. 2021, *MNRAS*, 501, 5597
- Hayden, M. R., Bovy, J., Holtzman, J. A., et al. 2015, *ApJ*, 808, 132
- Helmi, A., 2020, *ARA&A*, 58, 205
- Hirai, Y., Fujii, M. S., & Saitoh, T. R. 2021, *PASJ*, 73, 1036
- Hislop, J. M., Naab, T., Steinwandel, U. P., et al. 2022, *MNRAS*, 509, 5938
- Khoperskov, S., Haywood, M., Snaith, O., et al. 2021, *MNRAS*, 501, 5176
- Kobayashi, C., Umeda, H., Nomoto, K., Tominaga, N., Ohkubo, T., 2006, *ApJ*, 653, 1145
- Kovtyukh, V., Lemasle, B., Bono, G., et al. 2022, *MNRAS*, 510, 1894
- Leung, H. W. & Bovy, J. 2019, *MNRAS*, 489, 2079.
- Luck, R. E. & Lambert, D. L., 2011, *AJ*, 142, 136
- Mackereth, J. T. & Bovy, J. 2018, *PASP*, 130, 114501.
- Magrini, L. et al., 2016, *A&A*, 588, A91

- Magrini, L. et al., 2017, *A&A*, 603, A2
Majewski, S. R., et al., 2017, *AJ*, 154, 94
Méndez-Delgado, J. E., et al., 2022, *MNRAS*, 510, 4436
Naab, T., Ostriker, J. P., 2017, *ARA&A*, 55, 59
Palla, M., Matteucci, F., Spitoni, E., Vincenzo, F., & Grisoni, V. 2020, *MNRAS*, 498, 1710
Palla, M., 2021, *MNRAS*, 503, 3216
Palla, M., Santos-Peral, P., Recio-Blanco, A., Matteucci, F., 2022, *A&A*, 663, A125
Pignatari, M., Herwig, F., Hirschi, R., et al. 2016, *ApJS*, 225, 24
Queiroz, A. B. A., Anders, F., Chiappini, C. et al., 2020, *A&A*, 638, A76
Renaud, F., Agertz, O., Read, J. I., et al. 2021, *MNRAS*, 503, 5846
Ritter, C., Herwig, F., Jones, S., et al. 2018, *MNRAS*, 480, 538
Romano, D., Matteucci, F., Salucci, P., et al. 2000, *ApJ*, 539, 235
Rudolph, A. L., Fich, M., Bell, G. R., Norsen, T., Simpson, J. P., Haas, M. R., Erickson, E. F., 2006, *ApJS*, 162, 346
Schönrich, R., McMillan, P. J., 2017, *MNRAS*, 467, 1154
Somerville, R. S. & Davé, R. 2015, *ARA&A*, 53, 51
Spitoni, E., Silva Aguirre, V., Matteucci, F., et al. 2019, *A&A*, 623, A60
Spitoni, E., Cescutti, G., Minchev, I., et al. 2019, *A&A*, 628, A38
Spitoni, E., Verma, K., Silva Aguirre, V., et al. 2020, *A&A*, 635, A58
Spitoni, E., Verma, K., Silva Aguirre, V., et al. 2021, *A&A*, 647, A73
Spitoni, E., Aguirre Børsen-Koch, V., Verma, K., et al. 2022, *A&A*, 663, A174
Spitoni, E., Recio-Blanco, A., de Laverny, P., et al. 2022, arXiv:2206.12436
Stanghellini L., Haywood M., 2018, *ApJ*, 862, 45
Ting, Y.-S. & Rix, H.-W. 2019, *ApJ*, 878, 21
Vincenzo, F., Spitoni, E., Calura, F., Matteucci, F., Silva Aguirre, V., Miglio, A., Cescutti, G., 2019, *MNRAS*, 487, L47
Vincenzo, F., & Kobayashi, C. 2020, *MNRAS*, 496, 80
Vincenzo, F., Weinberg, D. H., Miglio, A., et al. 2021, *MNRAS*, 508, 5903
Yates, R. M., Henriques, B. M. B., Fu, J., et al. 2021, *MNRAS*, 503, 4474